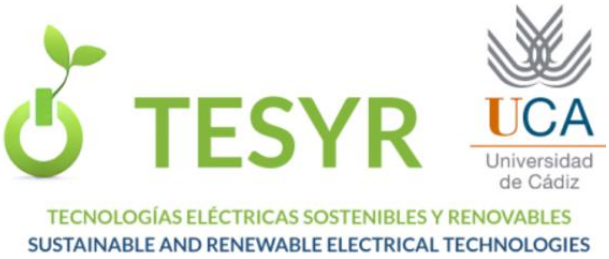

Universidad de Cádiz

Optimal Hierarchical Energy Management System for a Three-Bus Microgrid Cluster Configuration

Carrasco González, David; Hosseini, Ehsan; Sarrias Mena, Raúl; Horrillo Quintero, Pablo; García Triviño, Pablo; Fernández Ramírez, Luis Miguel

Published in:
2025 IEEE International Conference on Environment and Electrical Engineering and 2025 IEEE Industrial and Commercial Power Systems Europe, EEEIC / I and CPS Europe 2025

DOI (link to publication from Publisher):
Not available yet

Publication date:
Not available yet

Document Version:
Camera ready

Citation for published version (IEEE):
Not available yet

979-8-3315-9515-9/25/$31.00 ©2025 IEEE

Optimal Hierarchical Energy Management System for a Three-Bus Microgrid Cluster Configuration

David Carrasco-González
SURET Research Group
Department of Electrical Engineering
University of Cadiz
Algeciras, Spain
david.carrasco@uca.es

Ehsan Hosseini
SURET Research Group
Department of Electrical Engineering
University of Cadiz
Algeciras, Spain
ehsan.hosseini@uca.es

Raúl Sarrias-Mena
SURET Research Group
Department of Engineering in Automation, Electronics and Computer Architecture and Networks
University of Cadiz
Algeciras, Spain
raul.sarrias@uca.es

Pablo Horrillo-Quintero
SURET Research Group
Department of Electrical Engineering
University of Cadiz
Algeciras, Spain
pablo.horrillo@uca.es

Pablo García-Triviño
SURET Research Group
Department of Electrical Engineering
University of Cadiz
Algeciras, Spain
pablo.garcia@uca.es

Luis M. Fernández-Ramírez
SURET Research Group
Department of Electrical Engineering
University of Cadiz
Algeciras, Spain
luis.fernandez@uca.es

***Abstract*—The considerable research interest in microgrid clusters (MGCs) is owing to their ability to integrate diverse alternating current (AC) and direct current (DC) technologies for consumption, generation and storage, along with their inherent benefits in enhancing the reliability, efficiency, and resilience of energy systems. In this sense, this work presents a novel dynamic control for a grid-connected MGC, which includes an IEEE three-bus system interconnected with one DC microgrid (MG) (composed of a wind turbine, an ultracapacitor, electrical loads, a fuel cell, and an electrolyzer) and two AC MGs (composed each one of photovoltaic generators, electrical loads, and an electrical battery). The novel dynamic control consists of local controllers for each technology of the MGC and a dynamic hierarchical energy management system that coordinates an optimal power dispatch with the objective of optimizing the power losses in the transmission lines within the MGC. To evaluate the dynamic control, the system is studied under variations in the solar radiation, wind speed, and dynamic electrical loads. The dynamic control and the system exhibit robust behavior across the different simulation scenarios implemented.**

Keywords—Energy management system, IEEE three-bus system, losses, microgrid cluster, optimization

I. Introduction

The increasing use of renewable energy sources and the growing electricity demand are driving the development of microgrids (MGs) as autonomous, smarter and smaller energy systems [1]. These types of grids, with defined electrical limits and composed of renewable generation sources, energy storage systems (ESSs) and local consumers, offer economic, energy quality, and environmental benefits [2].

While MGs can operate autonomously, enabling their use in remote off-grid locations [3], they are frequently connected to a main grid to facilitate energy transfer when internal balance is difficult. Additionally, MGs can intentionally disconnect (island mode), necessitating self-sufficiency in energy generation, storage and consumption [4].

Initially, MGs relied on alternating current (AC) to ensure grid compatibility, but now they include direct current (DC) and hybrid configurations, enhancing operational flexibility [5]. In this situation, coordinating several adjacent MGs to create microgrid clusters (MGCs) provides easier integration of diverse technologies, local energy balancing, improved system performance (resilience, sustainability, efficiency and reliability), and promote decentralized energy generation and consumption [6].

To achieve operational goals in MG management, energy management systems (EMSs) are commonly implemented. Their primary function is to provide reference signals for the components of the MGs, which can be achieved through different methodologies [7], [8]. While [7] primarily focused on EMS for single MGs, there is a growing trend towards coordinated control strategies for MGCs. A limitation of many EMS currently is their focus on static systems with pre-defined strategies, thus neglecting dynamic operational variations in renewable energy or demand [8].

The use of advanced intelligent algorithms for EMSs has increased owing to their outstanding performance. In this sense, a fuzzy-logic EMS was used for a residential AC MG [9] and a model predictive EMS was used for an AC MG in [10] to optimize energy distribution while meeting the demand.

Among various advanced intelligent algorithms, optimizers demonstrated efficacy in addressing complex optimization problems, characterized by nonlinearities, multi-objectives and constraints [11], [12]. However, most of the proposed optimizers have been developed for single MGs, although they are slowly starting to be developed for hybrid AC-DC MGs, as mentioned in [12]. Regarding the development of optimizers for MGC, a multi-optimization EMS was developed for a MGC in [13], but the study is carried out with pre-defined strategies.

This work introduces a novel dynamic control strategy for a grid-connected MGC, which includes an IEEE three-bus system interconnected with one DC MG and two AC MGs and a dynamic hierarchical EMS that coordinates optimal power dispatch with the objective of optimizing the power losses on the transmission lines within the MGC.

The rest of the work is structured as follows. Section II presents the MGC model. The control system, specifically the optimal EMS, is described in Section III. Section IV provides the simulation results and their analysis. Finally, the conclusions of this work are presented in Section V.

This work was partially supported by Ministerio de Ciencia e Innovación, Agencia Estatal de Investigación, FEDER, UE (Grant PID2021-123633OB-C32 supported by MCIN/AEI/10.13039/501100011033/FEDER, UE).

II. System Configuration

The MGC structure is based on an IEEE three-bus system, where node 0 is linked to the main grid and an AC MG, node 1 to the other AC MG, and node 2 to the DC MG. Among the MGs, there are the transmission lines, as depicted in Fig. 1. The following subsections detail each technology employed in the system.

A. Main Grid

The MGC incorporates a stable AC main grid connected to node 0 of the IEEE three-bus system. This grid is modelled as an ideal three-phase AC voltage source without internal impedance and fixed frequency and voltage. In this work, the MGC is always in a grid-connected mode.

B. AC Microgrids

As shown in Fig. 1, the MGC incorporates two AC MGs within the IEEE three-bus system. One of them is connected to node 0 and the other one to node 1. Both AC MGs consist of a battery energy storage system (BESS), local electric loads, and photovoltaic (PV) generators connected to a common AC bus. To differentiate each AC MG, the technologies belonging to the AC MG connected to node 1 are labelled with number 1 after the name (e.g. PV1), and the technologies belonging to the other AC MG are labelled with number 2 (e.g. PV2).

The PV generators are modelled using an equivalent circuit comprising parallel resistors and diode, series resistors and a current source [14]. The PV generators are interfaced with the common AC bus using a boost converter and a voltage source inverter (VSI) [15]. These power converters elevate the DC voltage from the PV panels and convert the generated DC energy into AC for the common AC bus.

This work models a Li-ion BESS as a controlled voltage source and a series resistor. The BESS is interfaced with the common AC bus using a VSI.

Lastly, the AC MG is completed with two local electric loads per MG, configured as constant three-phase star connections. These loads are directly interfaced with the common AC bus using only circuit breakers.

C. DC Microgrid

As shown in Fig. 1, the MGC incorporates one DC MG in node 2 of the IEEE three-bus system. This MG employs an ultracapacitor (UC), a hydrogen system, electric loads, and a wind turbine (WT) connected to a common DC bus. Finally, the DC MG is interfaced with the AC bus of the system using a VSI.

The WT is represented by the sixth-order synchronous generator model [16]. The WT is interfaced with the common DC bus using an uncontrolled bridge rectifier and a boost converter. These power converters convert the generated AC energy into DC and elevate the DC voltage for the common DC bus.

The UC is modelled as an ideal capacitor and a series resistor. The UC is interfaced with the common DC bus using a half-bridge converter because this technology can generate and store energy.

The hydrogen system is composed of a fuel cell (FC) and an electrolyzer (EZ). The FC is modelled as a regulated voltage source and a diode; and the EZ is modelled as a voltage source and a series resistor. These technologies are interfaced with the common DC bus using a boost converter for the FC and a buck converter for the EZ. The first one is selected because the FC can only generate energy, and the second one is selected because the EZ can only store energy.

Lastly, the DC MG is completed with two constant electric DC loads. These loads are directly interfaced with the common DC bus using only circuit breakers.

III. Dynamic Control

The dynamic control system implemented in the MGC is composed of local controllers for each element of the MGC, and a dynamic hierarchical EMS that coordinates the optimal power dispatch to minimize the power losses in the transmission lines within the MGC. The following subsections detail the dynamic control implemented.

A. Local Controllers

The main grid, characterized by its stable frequency and voltage, does not require any local controller. Additionally, its inherent management of active and reactive power transfer with the MGC ensures the power balance and prevents frequency and voltage deviations.

The local loads in all MGs are managed via time-controlled circuit breakers for connection and disconnection to their respective buses, requiring no further control action.

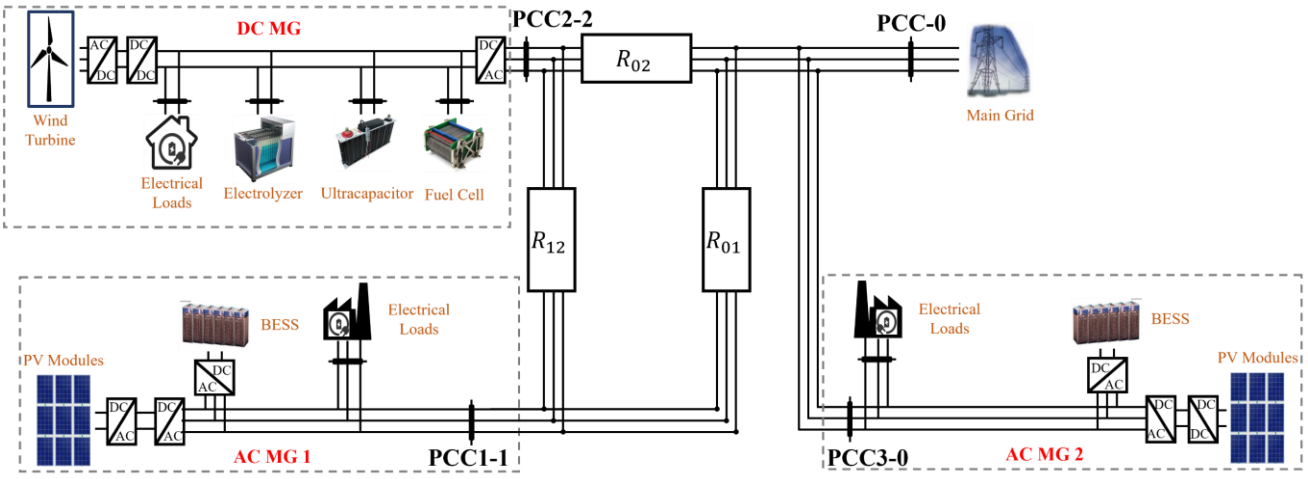

Fig. 1. System configuration.

In the case of the PV generators, the boost converter increases the voltage and enables the maximum power point tracking strategy using the Perturb & Observe algorithm. On the other side, the VSI regulates the voltage and frequency via a cascaded proportional-integral (PI) control loop to ensure the energy balance among the DC bus and the common AC bus.

The BESS utilizes a PI control loop to regulate active and reactive power transfer between the BESS and the system, ensuring proper DC-AC energy conversion for the common AC bus.

In the case of the WT, the uncontrolled bridge rectifier operates without control whereas the boost converter optimizes the WT performance by adjusting its speed according to wind speed variations.

For the ESSs used in the DC MG, PI controllers regulate the active power transfer for each ESS, ensuring that they track the references provided by the EMS. As there are three devices with different directions of the energy transfer, the UC controller allows generation and storage (positive and negative references, respectively), the FC allows energy generation (positive references) exclusively, and the EZ allows energy storage (negative references) exclusively.

Finally, the VSI that interfaces the DC MG to the common AC bus of the MGC is fundamental to stabilize and control the DC bus voltage against power fluctuations from variable wind speed and dynamic loads. Furthermore, this device converts DC energy from this MG to AC, enabling its integration in the IEEE three-bus system.

B. Hierarchical Energy Management System

In this work, an optimal and dynamic hierarchical EMS is developed and implemented to coordinate the optimal power dispatch of all elements of the MGC, in order to minimize the power losses in the transmission lines within the system and the energy transfer with the main grid, and ensure the ESSs safety via state-of-charge (SOC) monitoring. With these considerations, the EMS generates power references for all ESSs in the MGC

In this sense, the dynamic optimal EMS is structured into two different levels: 1) a centralized supervisory EMS, whose primary function is to ensure efficiently the energy balance and the optimization of the power losses in the transmission lines by controlling the energy transfer with the main grid and the different MGs; and 2) decentralized EMS in each MG, whose primary function is to ensure the energy balance of its own MG by adjusting the power reference of the ESSs.

1) Centralized supervisory EMS

This EMS operates based on the following inputs: the resistance of each transmission line (R_{01}, R_{02} and R_{12}), the SOC of each BESS (SOC_1 and SOC_3), the renewable generation of each MG (P_{GEN1} , P_{GEN2} and P_{GEN3}), the consumption of each MG (P_{CON1}, P_{CON2} and P_{CON3}), and the node voltages (V_0, V_1 and V_2).

Based on the above assumptions, the objective function for optimizing power losses in transmission lines is defined and calculated as the sum of the product of the resistance of each line and the squared current flowing through it. The current in each line is obtained by dividing the power flowing through that line (P_{01}, P_{02} and P_{12}) by the voltage difference between the extreme nodes:

$$min = \left\{\left(\frac{P_{01}}{V_0-V_1}\right)^2 \cdot R_{01} + \left(\frac{P_{02}}{V_0-V_2}\right)^2 \cdot R_{02} + \left(\frac{P_{12}}{V_1-V_2}\right)^2 \cdot R_{12}\right\} \quad (1)$$

P_{01} , P_{02} and P_{12} are the outputs of the optimization algorithm. However, the desired outputs of this EMS are the references of the active power transfers among the different MGs ($P_{1,\mathrm{r}}$, $P_{2,\mathrm{r}}$ and $P_{3,r}$). Therefore, these parameters are calculated through a power balance at each node, considering the sum of the active powers flowing in or out the node through the interconnection lines:

$$P_{1,r} = P_{12} - P_{01} \quad (2)$$

$$P_{2,r} = -P_{02} - P_{12} \quad (3)$$

$$P_{3,r} = P_{01} + P_{02} \quad (4)$$

The optimization algorithm in the EMS considers the SOC of the BESS for managing energy storage/release and the power limitations of the hydrogen system, potentially constraining their operation and ensuring the power balance in the MGC. In this work, these limitations are applied on the power constraints and the inequality restrictions of the algorithm.

As previously mentioned, the outputs of the algorithm are P_{01}, P_{02} and P_{12}. Therefore, these parameters are limited by the mentioned constraints.

The inequality restrictions are used to limit $P_{1,\mathrm{r}}$, $P_{2,\mathrm{r}}$ and $P_{3,r}$, and this is realized through (2), (3) and (4), as:

$$P_{1_{min}} \leq P_{12} - P_{01} \leq P_{1_{max}} \quad (5)$$

$$P_{2_{min}} \leq -P_{02} - P_{12} \leq P_{2_{max}} \quad (6)$$

$$P_{3_{min}} \leq P_{01} + P_{02} \leq P_{3_{max}} \quad (7)$$

where $P_{1_{min}}$, $P_{2_{min}}$ and $P_{3_{min}}$ are the minimum possible values of the active power transfers among the different MGs and $P_{1_{max}}$, $P_{2_{max}}$ and $P_{3_{max}}$ are the maximum possible values of the active power transfers among the different MGs.

The main objective of these limitations is to keep the ESS operating in safe conditions. Therefore, $P_{1_{min}}$, $P_{2_{min}}$, $P_{3_{min}}$, $P_{1_{max}}$, $P_{2_{max}}$ and $P_{3_{max}}$ are limited to the power usage of the ESSs of each MG. In this sense, each power limitation takes into account the power imbalance generated by the generated and consumed power of that MG, and the power limitation of the ESSs belonging to that MG.

For each AC MG, these boundaries are defined by the BESS capacity to store energy for the minimum limit, and the BESS capacity to release energy for the maximum limit. In the case of the DC MG, these power limitations are defined by the maximum power output of the EZ for the minimum limit, and the FC for the maximum.

The power constraints are used to limit P_{01}, P_{02} and P_{12}. To allow the power flow through the IEEE three-bus system, the maximum constraints of each transmission line (P_{max_T}) are limited to the summation of $P_{1_{max}}$, $P_{2_{max}}$ and $P_{3_{max}}$; and the minimum constraints (P_{min_T}) are limited to the

summation of $P_{1_{min}}$, $P_{2_{min}}$ and $P_{3_{min}}$, as shown in (8) and (9), respectively:

$$P_{max_T} = P_{1_{max}} + P_{2_{max}} + P_{3_{max}} \quad (8)$$

$$P_{min_T} = P_{1_{min}} + P_{2_{min}} + P_{3_{min}} \quad (9)$$

2) Decentralized EMS

At a lower hierarchical level, the EMS of each MG operates based on the following inputs: the generated and consumed power, and the active power transfers of its own MG. Based on these parameters, each EMS calculates the active power reference of the ESSs located in the MG as the difference between the active power transfer among that MG and its instantaneous power imbalance. For the AC MGs, the result of the difference is the active power reference of the BESS; and in the DC MG, the result is the active power reference of the EZ (if positive), or the active power reference of the FC (if negative).

Finally, regarding the EMS of the DC MG, the active power reference of the UC is calculated to handle the transitory power mismatches that the other slower ESSs in that MG cannot address. In this sense, this parameter is determined by the deviation of the actual power output of the FC and the EZ from their respective reference values. In this case, this EMS also receives as inputs the instantaneous output of the active power of the EZ and the FC to calculate this parameter.

IV. Evaluation of the Simulation Results

To evaluate the designed dynamic control and MGC, a 100-second simulation is conducted using Simulink (version 10.5), a component of MATLAB 2022a. The SimPowerSystems library in Simulink is employed to implement the dynamic MGC, while the fmincon solver, via an embedded function, is used for the dynamic hierarchical EMS. Finally, Simulink employes the ode14x solver, configured as fixed-step type, to execute the simulation.

Different operating conditions driven by different inputs are modelled, consisting of variations in the incident solar radiation for each PV generator and wind speeds, and dynamic connection/disconnection of the local loads. Finally, the initial SOC of both BESSs is set to 50%, representing two more operational inputs.

Fig. 2 presents the power generated and consumed in the system. The wind speeds variations modulate the WT power generation, while the power generated by each of the two PV generators are driven by the changes in their incident solar radiation. A similar situation occurs with the modifications in the power demand profile of the local loads, which vary based on the connection/disconnection of the loads to the MGs.

While all the local loads are modeled as constant values, the DC load profile exhibits lower fluctuations. These variations in the DC loads are produced by the voltage fluctuations in the DC bus. The AC load profiles do not exhibit this effect because the main grid ensures a steady voltage on the AC buses. A similar behavior is observed in the WT power generation.

Fig. 3 illustrates the active power transfers among the different MGs (P_1, P_2 and P_3), their respective references and the active power transfer with the main grid (P_{PCC}). As

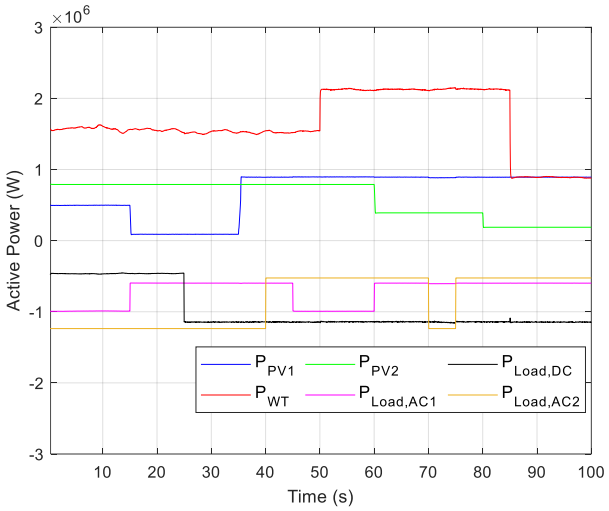

Fig. 2. Generated and consumed power in the system.

depicted, all the parameters perfectly track their respective references provided by the centralized supervisor EMS, even though these parameters are indirectly controlled by power transfer inside each MG. During most of the simulation, the algorithm determines that P_1, P_2 and P_3 are almost zero to optimize the power losses in the transmission lines. Therefore, the power generated in each MG is stored or consumed in the same MG. However, there are two time intervals (between 0 and 25 s, and from 70 s to 75 s) when this is not true. These can occur because one of the MGs cannot maintain the energy balance with their ESSs, and the algorithm determines what

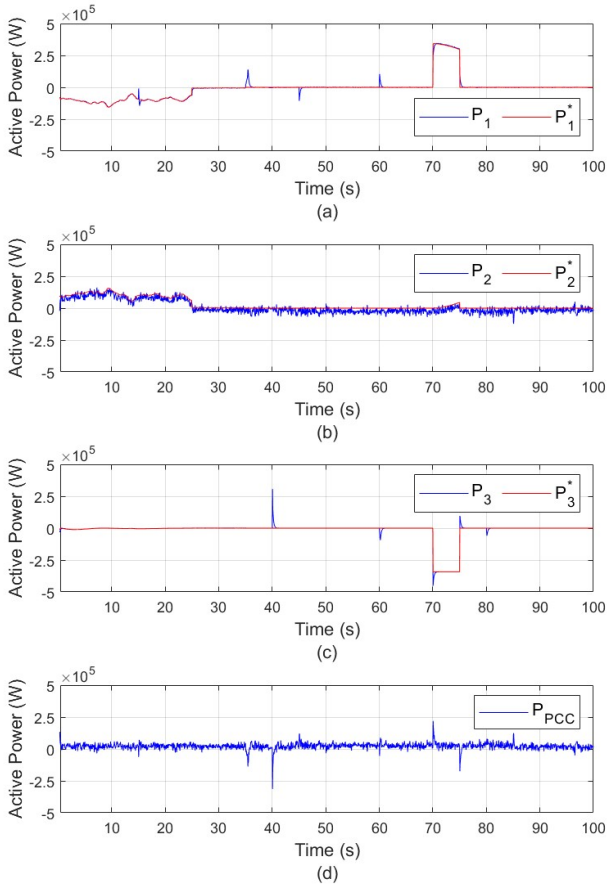

Fig. 3. Active power transfer among the system: (a) AC MG 1, (b) DC MG, (c) AC MG 2 and (d) main grid.

MG generates a lower power loss having into account the SOC of the ESSs.

Additionally, the main grid interacts with the system to maintain the power balance when there are changes in the operating conditions of the MGC. In addition, the main grid supplies or absorbs the difference in energy that the MGs cannot handle to maintain the power balance. When the powers are balanced, the power transfer with the main grid decreases to a negligible level. Therefore, the optimal hierarchical EMS manages to adjust the power transfer among MGs to minimize the dependence on the main grid.

Fig. 4 presents the active power transfer among the ESSs and their respective references. As depicted, all the ESSs perfectly track their respective references provided by the decentralized EMSs. Between 0 and 25 s, the EZ of the DC MG reaches its maximum power capacity, generating a power transfer in that MG (P_2) which is stored in the BESS1. Between 70 and 75 s, the BESS2 reaches its maximum power capacity, owing to its 50% SOC, generating a power transfer

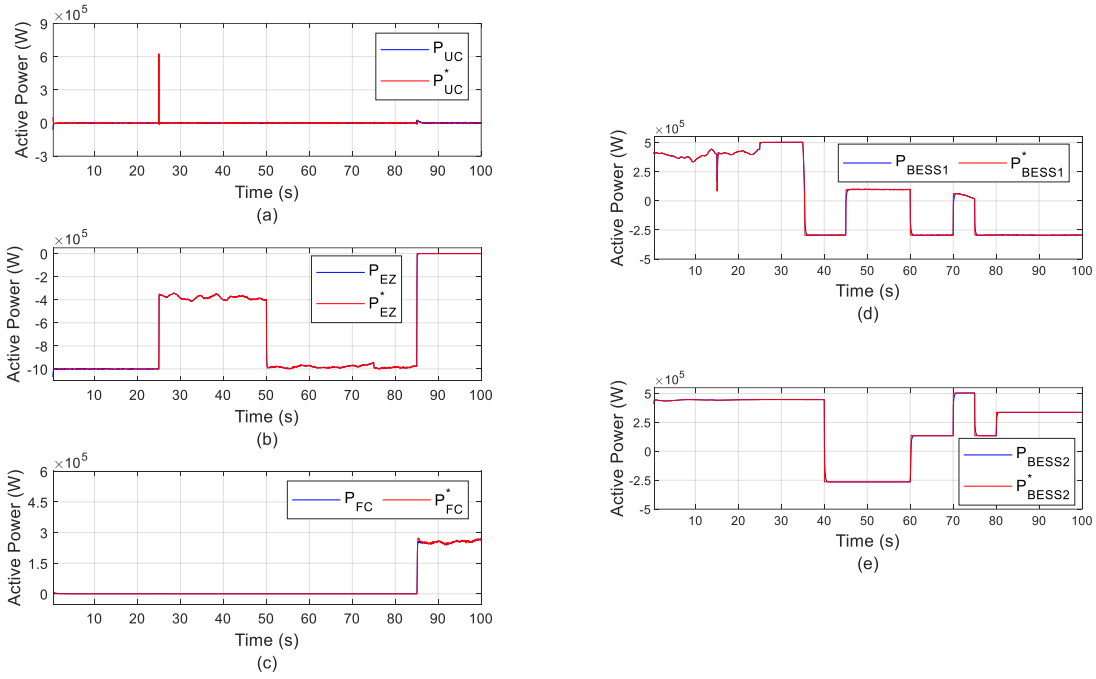

Fig. 4. Active power transfer among the ESSs and their references: (a) UC, (b) EZ, (c) FC, (d) BESS1 and (e) BESS2.

in that MG (P_3) that is provided by the BESS1. In the rest of the situations, the ESSs of each MG cover the references of P_1, P_2 and P_3 provided by the centralized supervisory EMS.

Finally, the UC can manage transitory power mismatches in the DC MG, with significant power peaks. Its output power approaches zero as the other ESSs of the DC MG stabilize.

Fig. 5 illustrates the active power losses produced in the transmission lines ($P_{L,01}$, $P_{L,02}$ and P_{L12}) and the sum of all the active power losses in the system ($P_{L,T}$). As depicted, the lack of power transfer among the MGs leads to lower losses. On the other hand, when power transfer among the different MGs is necessary, because they cannot be self-sufficient, the active power losses are higher. In these cases, the optimizer calculates which MG can cover this power imbalance with minimum power losses, considering the constraints of the problem. Furthermore, $P_{L,01}$ is higher than $P_{L,02}$ and $P_{L,12}$ because that line has a higher impedance. The power profile indicates a total energy loss of 0.076 kWh over this simulation. This translates to an average power loss of 2650 W, which is considerably small when compared to the typical power levels within the system.

Fig. 6 illustrates presents the DC bus voltage in the DC MG, which is effectively regulated around its 1100 V reference. This control is essential for the correct operation of the DC MG and its components. Although fluctuations occurred due to the EZ, FC and UC operation, DC load connection/disconnection, and WT output variations, the local VSI controller successfully maintained the DC bus voltage at the mentioned reference.

The results presented in this section indicate a robust performance across the different scenarios simulated and a satisfactory operation of the proposed dynamic control and the system.

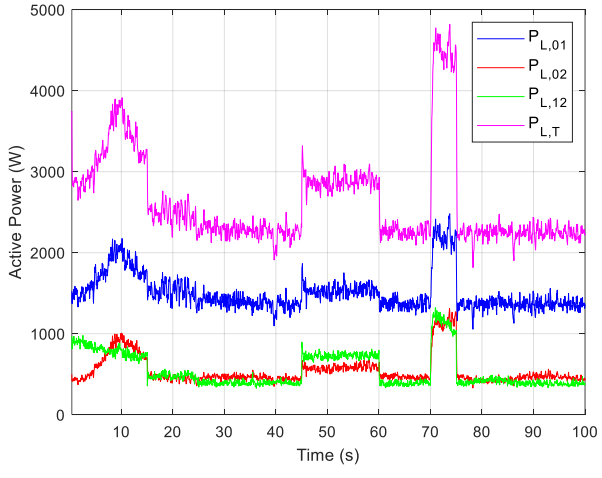

Fig. 5. Active power losses in each transmission line and the total active power losses of the system.

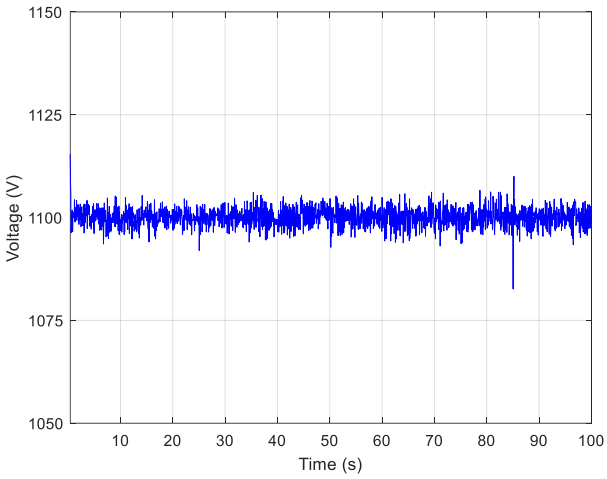

Fig. 6. Voltage of the DC MG.

V. Conclusions

This work presented a novel dynamic control for a grid-connected MGC, consisting of an IEEE three-bus system interconnected with one DC MG and two AC MGs. The DC MG included a WT, local DC loads, an EZ, a FC and an UC; whereas each AC MG included PV generators, local AC loads and an electrical BESS. The dynamic operation of these different technologies, each one with its unique operational characteristics, demonstrated the potential of MGC to enhance grid stability and energy efficiency.

The novel dynamic control consisted of local controllers for each component of the MGC, and a dynamic hierarchical EMS that coordinates an optimal power dispatch to optimize the power losses in the transmission lines within the MGC. Additionally, the EMS minimized the power transfer with the main grid and ensured the correct usage of the ESSs.

The proposed dynamic control and the MGC were tested under a range of different scenarios. The simulation results confirmed their robustness and effectiveness under these dynamic scenarios. In this sense, the EMS perfectly adapted to the dynamic scenarios in renewable generation and demand, a key advantage over static EMS approaches.

Additionally, the dynamic control had a satisfactory operation, achieving the objectives set in this work, where the power transfer with the main grid was minimal, so minimizing the active power losses. These findings underscore the potential of the proposed dynamic control to significantly enhance the efficiency and reliability of the MGC in an IEEE three-bus system, offering a valuable contribution to this field.

References

[1] S. Howell, Y. Rezgui, J. L. Hippolyte, B. Jayan, and H. Li, "Towards the next generation of smart grids: Semantic and holonic multi-agent management of distributed energy resources," *Renewable and Sustainable Energy Reviews*, vol. 77, pp. 193–214, Sep. 2017, doi: 10.1016/J.RSER.2017.03.107.

[2] L. Mariam, M. Basu, and M. F. Conlon, "Microgrid: Architecture, policy and future trends," *Renewable and Sustainable Energy Reviews*, vol. 64, pp. 477–489, Oct. 2016, doi: 10.1016/J.RSER.2016.06.037.

[3] Y. Li, R. Wang, and Z. Yang, "Optimal Scheduling of Isolated Microgrids Using Automated Reinforcement Learning-Based Multi-Period Forecasting," *IEEE Trans Sustain Energy*, vol. 13, no. 1, pp. 159–169, Jan. 2022, doi: 10.1109/TSTE.2021.3105529.

[4] F. S. Al-Ismail, "DC Microgrid Planning, Operation, and Control: A Comprehensive Review," *IEEE Access*, vol. 9, pp. 36154–36172, 2021, doi: 10.1109/ACCESS.2021.3062840.

[5] Pragya and R. Thakur, "A Review of Architecture and Control Strategies of Hybrid AC/DC Microgrid," *2022 International Conference on Intelligent Controller and Computing for Smart Power, ICICCSP 2022*, 2022, doi: 10.1109/ICICCSP53532.2022.9862386.

[6] B. Chen, J. Wang, X. Lu, C. Chen, and S. Zhao, "Networked Microgrids for Grid Resilience, Robustness, and Efficiency: A Review," Jan. 01, 2021, *Institute of Electrical and Electronics Engineers Inc.* doi: 10.1109/TSG.2020.3010570.

[7] A. R. Abbasi and D. Baleanu, "Recent developments of energy management strategies in microgrids: An updated and comprehensive review and classification," *Energy Convers Manag*, vol. 297, p. 117723, Dec. 2023, doi: 10.1016/J.ENCONMAN.2023.117723.

[8] T. Sattarpour, S. Golshannavaz, D. Nazarpour, and P. Siano, "A multi-stage linearized interactive operation model of smart distribution grid with residential microgrids," *International Journal of Electrical Power & Energy Systems*, vol. 108, pp. 456–471, Jun. 2019, doi: 10.1016/J.IJEPES.2019.01.023.

[9] J. Wu *et al.*, "Hierarchical online energy management for residential microgrids with Hybrid hydrogen–electricity Storage System," *Appl Energy*, vol. 363, p. 123020, Jun. 2024, doi: 10.1016/J.APENERGY.2024.123020.

[10] P. Horrillo-Quintero, P. García-Triviño, R. Sarrias-Mena, C. A. García-Vázquez, and L. M. Fernández-Ramírez, "Model predictive control of a microgrid with energy-stored quasi-Z-source cascaded H-bridge multilevel inverter and PV systems," *Appl Energy*, vol. 346, p. 121390, Sep. 2023, doi: 10.1016/J.APENERGY.2023.121390.

[11] J. M. Raya-Armenta, N. Bazmohammadi, J. G. Avina-Cervantes, D. Sáez, J. C. Vasquez, and J. M. Guerrero, "Energy management system optimization in islanded microgrids: An overview and future trends," *Renewable and Sustainable Energy Reviews*, vol. 149, p. 111327, Oct. 2021, doi: 10.1016/J.RSER.2021.111327.

[12] E. Hernández-Mayoral *et al.*, "A Comprehensive Review on Power-Quality Issues, Optimization Techniques, and Control Strategies of Microgrid Based on Renewable Energy Sources," *Sustainability 2023, Vol. 15, Page 9847*, vol. 15, no. 12, p. 9847, Jun. 2023, doi: 10.3390/SU15129847.

[13] M. Roustaee and A. Kazemi, "Multi-objective energy management strategy of unbalanced multi-microgrids considering technical and economic situations," *Sustainable Energy Technologies and Assessments*, vol. 47, p. 101448, Oct. 2021, doi: 10.1016/J.SETA.2021.101448.

[14] M. A. Hasan and S. K. Parida, "An overview of solar photovoltaic panel modeling based on analytical and experimental viewpoint," *Renewable and Sustainable Energy Reviews*, vol. 60, pp. 75–83, Jul. 2016, doi: 10.1016/J.RSER.2016.01.087.

[15] A. Yazdani and I. Reza, *Voltage source converter in power system*. 2010. Accessed: Jul. 28, 2023. [Online]. Available: https://www.wiley.com/en-ca/Voltage+Sourced+Converters+in+Power+Systems+%3A+Modeling%2C+Control%2C+and+Applications-p-9780470521564

[16] E. Hosseini *et al.*, "Optimal energy management system for grid-connected hybrid power plant and battery integrated into multilevel configuration," *Energy*, vol. 294, p. 130765, May 2024, doi: 10.1016/J.ENERGY.2024.130765.